Diurnal Variations of Warm-Season Precipitation over Northern China

HUIZHONG HE

State Key Laboratory of Severe Weather, Chinese Academy of Meteorological Sciences, Beijing, China, and Department of Meteorology, The Pennsylvania State University, University Park, Pennsylvania

FUQING ZHANG

Department of Meteorology, The Pennsylvania State University, University Park, Pennsylvania

(Manuscript received 22 January 2010, in final form 12 February 2010)

ABSTRACT

This study examines the diurnal variations of the warm-season precipitation over northern China using the high-resolution precipitation products obtained from the Climate Prediction Center's morphing technique (CMORPH) during May–August of 2003–09. The areas of focus are the Yanshan–Taihangshan Mountain ranges along the east peripheries of the Loess and Inner Mongolian Plateaus and the adjacent North China Plains. It is found that the averaged peak in local precipitation begins early in the afternoon near the top of the mountain ranges and propagates downslope and southeastward at a speed of $\sim$13 m s^{-1}. The peak reaches the central North China Plains around midnight and the early morning hours resulting in a broad area of nocturnal precipitation maxima over the plains. The diurnal precipitation peak (minimum) is closely collocated with the upward (downward) branch of a mountain–plains solenoid (MPS) circulation. Both the MPS and a low-level southwesterly nocturnal jet are likely to be jointly responsible for the nighttime precipitation maxima over the plains.

1. Introduction

Diurnal variations of precipitation are very important to the local and global weather and climate, which can have strong implications on the hydrological cycle and agriculture. For example, summertime rainfall may evaporate more quickly in the afternoon hours but can easily be permeated into soil and stored overnight. Numerous past studies have examined the diurnal variations of global and regional rainfalls through observations from surface rain gauges, weather radars, and/or satellites (e.g., Wallace 1975; Carbone et al. 2002; Yu et al. 2007; Wang et al. 2004; Dai et al. 1999, 2007; Zhou et al. 2008; Chen et al. 2009; Yin et al. 2009). It is commonly observed that warm-season precipitation around the world usually peaks in the morning over ocean and in the late afternoon over land with the exception of several low-lying land areas such as the central Great Plains of the United States (e.g., Wallace 1975; Carbone et al. 2002). Some studies partially accredit the nocturnal precipitation maximums over the plains to a low-level southerly nocturnal jet parallel (e.g., Higgins et al. 1997; Carbone and Tuttle 2008), which is also widely observed over the Great Plains of the United States (e.g., Bonner 1968).

Complementary to Carbone et al. (2002), which concentrated on the central United States, the current study explores the diurnal variation and propagation of the warm-season precipitation over the Yanshan–Taihangshan Mountain ranges, along the eastern peripheries of the Loess and Inner-Mongolian Plateaus and the adjacent North China Plains (Fig. 1a). Warm-season rainfalls account for nearly 80% of the total annual precipitation in this focus area, which has strong diurnal variations. This study also complements recent studies on diurnal rainfall variations over China (e.g., Wang et al. 2004; Yu et al. 2007; Zhou et al. 2008; Chen et al. 2009), most of which emphasize the eastern slopes and adjacent eastward regions of the Tibetan Plateau.

Corresponding author address: Dr. Fuqing Zhang, Department of Meteorology, The Pennsylvania State University, University Park, PA 16802.
E-mail: fzhang@psu.edu

DOI: 10.1175/2010MWR3356.1

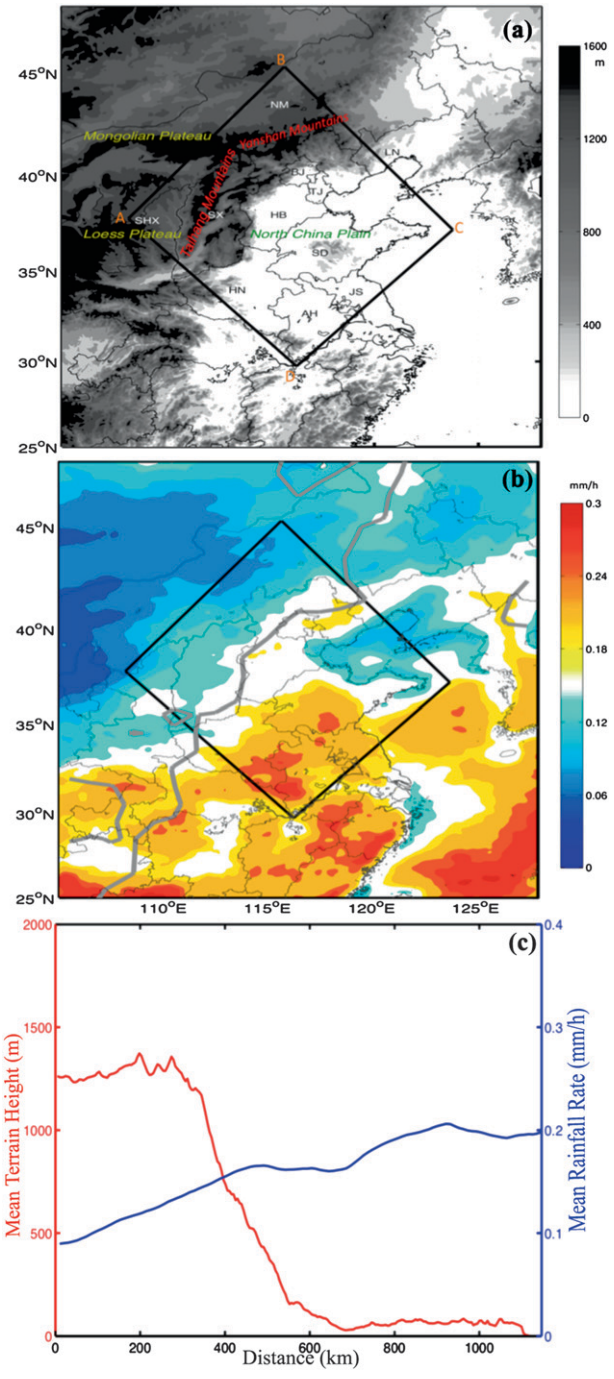

FIG. 1. (a) Study domain map and terrain distribution (shaded every 200 m) over northern China with the focus area highlighted in box ABCD, which includes the cities of Beijing (denoted as BJ) and Tianjin (TJ) and the provinces of Shanxi (SX), Inner-Mongolia (NM), Hebei (HB), Shandong (SD), Henan (HN), Anhui (AH), and Jiangsu (JS). (b) Distribution of mean warm-season hourly rainfall rate (mm h^{-1}) averaged over all hours from May to August during 2003–09 estimated with the CMORPH dataset. (c) Averaged terrain elevation and hourly precipitation rate along the northwest–southeast direction averaged over the boxed area in (a). The starting point of the cross section is an average over line AB, and the ending point is an average over line CD; the same averaging method will be used for Figs. 4 and 6 along the same cross section.

2. Precipitation dataset and mean

The high-resolution global precipitation dataset from the National Oceanic and Atmospheric Administration (NOAA) Climate Prediction Center's morphing technique (CMORPH; Joyce et al. 2004) will be used for this study. The CMORPH has a spatial resolution of 0.7277° and is available every 30 min between 60°N and 60°S beginning with December of 2002. It combines precipitation estimates derived exclusively from several low-orbiter satellite microwave sensors. During periods when microwave data are not available at a location, it uses spatial propagation information obtained from geostationary satellite infrared data to transport the microwave-derived precipitation features (see more technical details online at http://www.cpc.noaa.gov/products/janowiak/cmorph_description.html).

This study examines CMORPH data over all available warm-season months (May–August) during 2003–09 on a 23° × 23° domain (25°–48°N, 105°–128°E; Fig. 1a). The NOAA Global Forecast System (GFS) 1° × 1° operational analyses, available every 6 h over the course of this period, are used to provide the corresponding environmental conditions.

Our focus area is over the Yanshan–Taihangshan Mountain ranges along the east peripheries of the Loess–Mongolian Plateaus and the adjacent North China Plains (Fig. 1a), which have similar terrain patterns to that studied in Carbone et al. (2002, see their Fig. 1b) with the exception of predominant slope declines that transverse from northwest to southeast in northern China instead of from west to east over the Rocky Mountains and adjacent Great Plains of the United States. The prevailing warm-season midtropospheric steering-level winds over the area of focus are predominantly northwesterly from high terrains to lower plains (not shown).

Averaged over all warm-season hours from May to August during 2003–09, the total precipitation over the North China Plains on the southeastern side of the domain is much higher than that over the plateaus to the northwest (Fig. 1b). The rainfall distribution from the CMORPH estimate agrees well with the rain gauge observations (e.g., Qian et al. 2002, their Fig. 1), which adds confidence to the applicability of the CMORPH dataset as attested by Janowiak et al. (2005), Dai et al. (2007), and Zhou et al. (2008).

Figure 1c shows the mean terrain and precipitation along the northwest–southeast direction averaged over the boxed focus area in Fig. 1a. A sharp drop in elevation of more than 1200 m from ~250 to 550 km exists. On average, the higher the terrain is the lower is the warm-season precipitation amount. The averaged precipitation rate increases by nearly a factor of 2 from the top of

the plateaus (on the northwest) to the flat plains (on the southeast).

3. The diurnal precipitation cycle and its phase propagation

Figure 2a shows the spatial distribution of the diurnal contribution to total precipitation, expressed as a percentage (i.e., diurnal component divided by the mean hourly precipitation rate). The diurnal component is calculated by summing the absolute differences between the mean precipitation rate at each hour and the mean hourly precipitation rate. Differing from the total rainfall distribution in Fig. 1b, the highest percentage of diurnal precipitation occurs along the sharp terrain slope that makes a transition from the low plains to the high plateaus, and the lowest percentage of diurnal precipitation occurs over the plains. Figure 2b shows isochrones of the local diurnal precipitation peaks that summarize the location of the phase fronts of diurnal precipitation peaks for different hours in that are shown in Fig. 3. As motivated by Fig. 12 of Carbone et al. (2002), Fig. 4 shows the distance–time Hovmöller diagram of the normalized hourly precipitation deviations averaged along a cross section from northwest to southeast (as in Fig. 1c). To highlight the larger-scale variations of diurnal precipitation peaks and to compare directly with a coarse GFS analysis that will be shown in Figs. 5 and 6, a two-dimensional spectral decomposition (Lin and Zhang 2008) has been used to filter signals with horizontal scales of less than 300 km in Figs. 2b and 3, but no filtering is performed in Fig. 4.

Figures 2b, 3, and 4 show that a local diurnal precipitation peak starts in early afternoon hours (with maximum solar heating) on or near the top of the Yanshan–Taihangshan Mountain ranges. The strongest local diurnal peak is observed on the sharpest terrain slope east of the plateaus in the midafternoon hours [between 1400 and 1700 Beijing time, i.e., the local standard time (LST), which is 8 h ahead of UTC; Fig. 4], which subsequently moves downslope toward the southeast (Figs. 2b and 4). The peak phase arrives on the plains in late afternoon into the early evening (Fig. 3c) and continuously progresses eastward across the central plains throughout the night (Figs. 3d,e). It approaches the eastern edges of the focus domain at around 0000 UTC (0800 LST), but by this time the diurnal peak begins to lose its identity while daylight returns the next morning (Fig. 3f). There also exists a secondary precipitation maximum over the eastern plains during the late afternoon hours (Figs. 3b–d and 4), implying a semidiurnal rainfall cycle over these areas as was also noted by Yu et al. (2007).

The averaged phase propagation speed toward the southeast starting from the top of the mountain ranges is approximately 13 m s^{-1}, which is similar to that of a 14 m s^{-1} eastward speed in Carbone et al. (2002, their Fig. 2), except that the phase propagation is more coherent in the current study (Fig. 4). Note that Fig. 4 also shows the presence of two parallel, smaller-scale peaks within the primary diurnal peak phase in the plains, separated by ~100 km in horizontal distance and ~3 h in time, which is not visible in the filtered maps in Fig. 3. Parallel to the diurnal precipitation peak phase line, there is also a southwest–northeast belt of daily precipitation minimum visible at nearly all hours. The minimum phase is most pronounced at the top the Yanshan–Taihangshan Mountain ranges right after midnight, at the sharpest terrain slope during early morning hours, and on the plains in the late morning through early afternoon hours (Figs. 3 and 4).

4. Discussion on diurnal propagation and nocturnal precipitation peaks

The speed of phase propagation and the relationship between the local diurnal precipitation maxima and minima may be related to the diurnal variation of a regional-scale, mountain–plains solenoid (MPS) circulation induced by differential heating between the high mountain ranges and the plains over this region. This is evident by examining the mean GFS analysis averaged through the same warm-season months of 2003–09 shown in Figs. 5–6. The evolution of the MPS circulation over the Rocky Mountains and the adjacent plains of the United States, along with its impacts on summertime precipitation and other weather phenomena, has been extensively studied (e.g., Tripoli and Cotton 1989; Wolyn and McKee 1994; Zhang and Koch 2000; Koch et al. 2001; Carbone and Tuttle 2008).

Figure 5 shows the low-level (900 hPa) vertical motions and perturbation wind vectors at each GFS analysis averaged over 2003–09. Figure 6 shows the corresponding averaged vertical motions, or the perturbation vertical circulation vectors averaged along the same northwest–southeast cross section as in Figs. 1c and 4. Note that the 900-hPa pressure surface in some high-mountain areas is slightly below the ground level, but the GFS analysis from the downward extrapolation depicts reasonably well the low-level flow patterns in these places.

At 0600 UTC (1400 LST) in the early afternoon, there are widespread low-level upward motions on the plateaus that peak on the eastern edge along the Yanshan–Taihangshan Mountain ranges (Figs. 5a and 6a). This peak quasi-southwest–northeast-oriented upward motion belt is closely collocated with a low-level perturbation

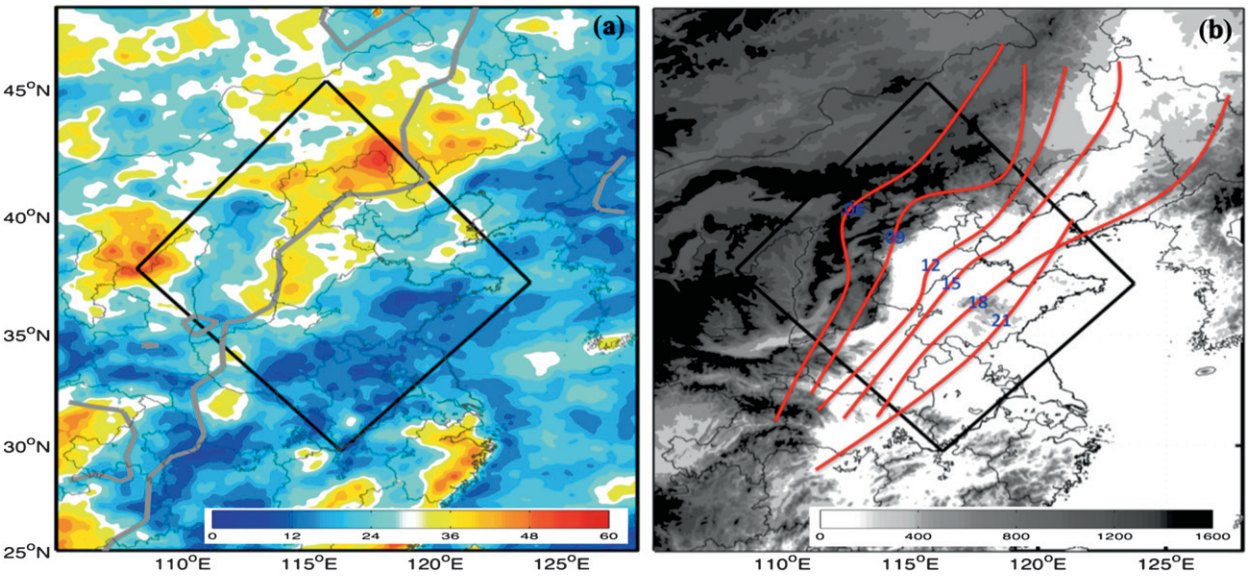

FIG. 2. (a) Percentage of the diurnal contributions of the total precipitation (calculated as the sum of the absolute differences between the mean precipitation rate at each hour and the mean hourly precipitation rate divided by the mean hourly precipitation rate). The 800-m terrain elevation is plotted in thick gray curves denoting the approximate location of the steepest terrain slope. (b) Isochrones (phase fronts) of the local diurnal precipitation peaks at different times of Fig. 3 with terrain elevations shaded every 200 m. The time label of the isochrones in (b) is in UTC [i.e., 8 h behind the local standard time (Beijing time)].

convergence boundary, both of which correspond to be the upward branch of a developing daytime MPS (Fig. 6a) that is likely responsible for the peak diurnal precipitation in this area (Fig. 3a). The downward branch of the MPS circulation along with the cold-air advection by the anomalous low-level northeasterly winds (Figs. 5a and 6a) is likely responsible for the diurnal precipitation minimum phase across the plains at this time (Fig. 3a).

At 1200 UTC (2000 LST) in the early evening, the maximum upward motion belt is located on the eastern slopes and foothills of the Yanshan–Taihangshan Mountain ranges, where the perturbation low-level winds from the low plains are being lifted upward by the steepest terrain slopes (Figs. 5b and 6b). As part of the upward branch of the MPS circulation, the upslope lifting induces the strongest diurnal precipitation peaks along the terrain slopes and foothills at this hour (Figs. 2a and 3c). In the meantime, the eastern half of the plains is positioned under the downward branch of the MPS, which adversely affects precipitation. Also at this time, the top of the mountain ranges makes a transition toward downward motions and shifts to the minimum diurnal precipitation phase (Figs. 3c and 5b).

At 1800 UTC (0200 LST) in the early morning, the upward branch of the MPS circulation moves to the central plains along a leeside convergence zone (Figs. 5c and 6c) that collocates well with a nocturnal precipitation maximum (Fig. 3e). Meanwhile, because of the decrease of boundary layer friction and turbulent mixing that results in the absence of solar heating, a perturbation low-level southwesterly nocturnal jet has fully developed (Figs. 5c and 6c). This enhances the low-level warm-, moist-air advection from the southwest as well as low-level lifting, both of which are likely responsible for the nocturnal precipitation maximum over the plains (Fig. 3e). By now, strong downslope flows (Fig. 6c) have led to a precipitation minimum over the slopes and foothills (Fig. 3e). A low-level southerly nocturnal jet, parallel to the mountain ranges, is also widely observed over the Great Plains of the United States (e.g., Bonner 1968) and has at least in part been a cause of nocturnal precipitation maxima (e.g., Higgins et al. 1997).

At 0000 UTC (0800 LST), a few hours after sunrise, the upward branch of the remnant MPS circulation remains over the central plains but is substantially weakened while the perturbation low-level southwesterly jet has been completely replaced by the north-northwesterly downslope winds (Figs. 5d and 6d). There is only a very weak signature of the diurnal precipitation peak associated with this upward branch. The minimum precipitation phase is observed over most of the focus domain, except at the eastern corner where the ocean has a strong influence (Fig. 3f).

The above diagnosis performed with the GFS analysis demonstrates a strong connection between the evolution of peak diurnal precipitation and the upward branch of an

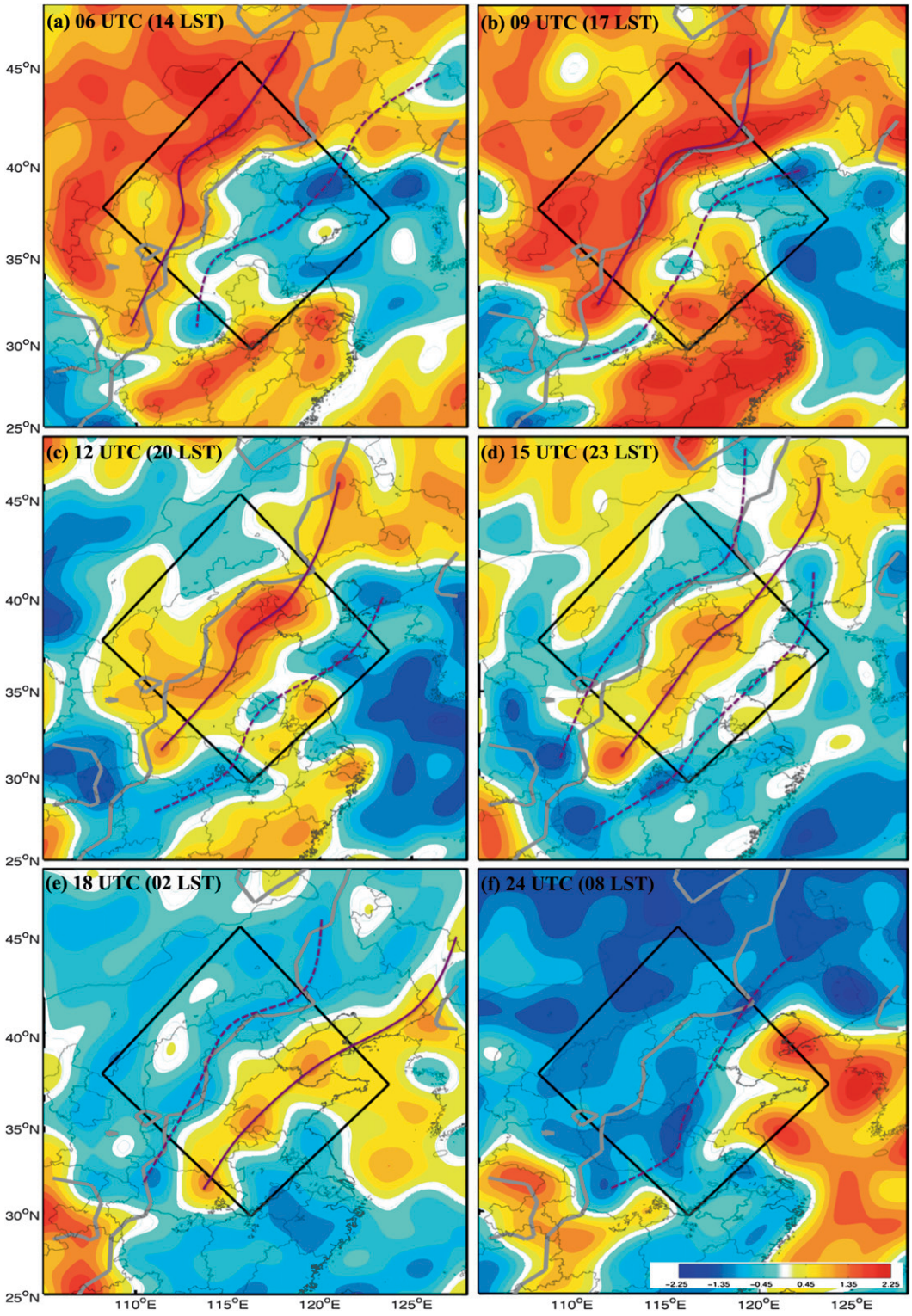

FIG. 3. Map distribution of normalized diurnal precipitation deviations at (a) 0600, (b) 0900, (c) 1200, (d) 1500, (e) 1800, and (f) 0000 UTC estimated as the mean precipitation rate at this hour minus the mean precipitation rate throughout the date, normalized by the standard deviation of hourly precipitation at each location. Scales smaller than 200 km are truncated by a 2D spectral decomposition. The 800-m terrain elevation is plotted in thick gray curves denoting the approximate location of the steepest terrain slope. The purple solid (dashed) line denotes the location of the phase fronts of the local diurnal precipitation peaks (minima).

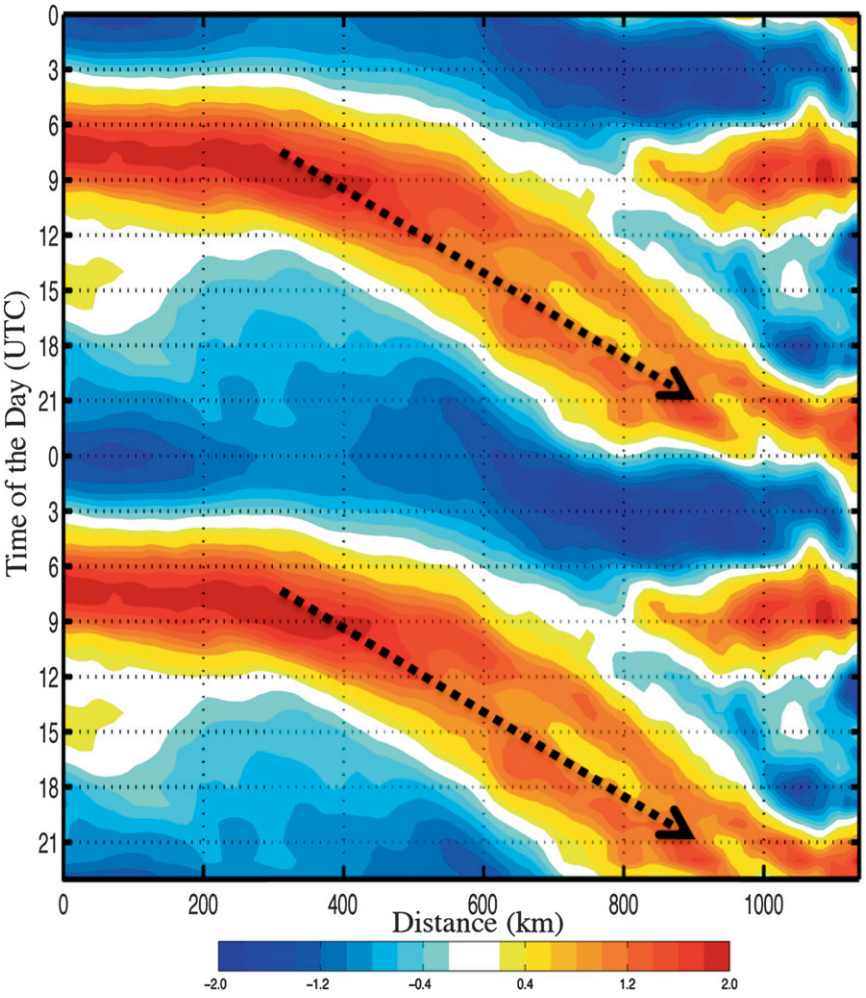

FIG. 4. Distance–time Hovmöller diagram of the normalized hourly precipitation deviation without filtering averaged along the cross section from northwest to southeast (as in Fig. 1c). The dashed arrows show the southeastward phase propagation of the diurnal precipitation peaks. The time axis is in UTC [i.e., 8 h behind the local standard time (Beijing time)].

MPS circulation, progressing southeastward from the top of the mountain ranges in the early afternoon to the central North China Plains in the early morning. The 13 m s^{-1} propagation speed and direction correspond to a midtropospheric steering level at around 500 hPa (not shown).

There exist at least two possible mechanisms responsible for the nocturnal precipitation maximum over the plains, related to the MPS circulation: 1) the initiation or enhancement of precipitation events in the afternoon on the top and/or eastern slopes of the mountain ranges that subsequently propagate southeastward to the plains, following the midtropospheric mean flow, and 2) the local initiation or enhancement of precipitation following the upward branch of the MPS circulation over the plains during the night, which is further enhanced by the low-level southwesterly nocturnal jet.

However, given the coarse spatial and temporal resolution of the GFS analysis (1° × 1°, every 6 h), the causality between the upward branch of the MPS and the precipitation maxima cannot be uniquely determined. It remains possible that the nighttime upward motion over the plains (e.g., Figs. 5c and 6c) results from (instead of causing) the nocturnal precipitation maxima.

There is spatial and temporal separation between the two parallel subpeaks within the primary diurnal precipitation maximum over the plains. The maximum to the east may have been produced by secondary generation of convection ahead of the downslope-sliding convective lines through either mesoscale gravity waves

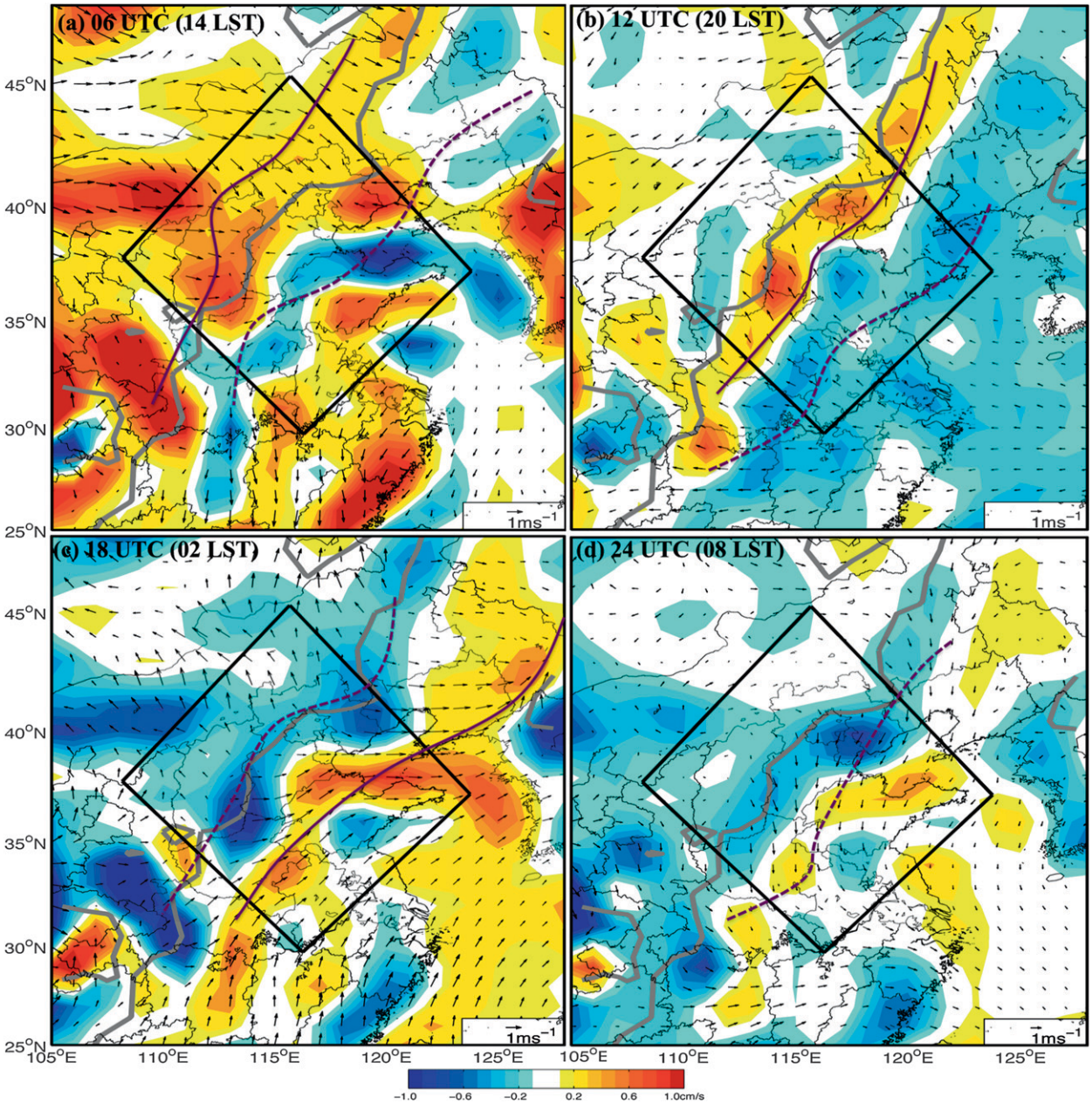

FIG. 5. Spatial distribution of the 900-hPa vertical motions (colored) and perturbation wind vectors diagnosed with the GFS analyses at (a) 0600, (b) 1200, (c) 1800, and (d) 0000 UTC. The 800-m terrain elevation is plotted in thick gray curves denoting the approximate location of the steepest terrain slope. The purple solid (dashed) line denotes the location of the phase fronts of the local diurnal precipitation peaks (minima) as in Fig. 3.

and/or cold-pool dynamics as hypothesized in Carbone et al. (2002) and Trier et al. (2006, 2010).

5. Conclusions

This study explores the diurnal variations of warm-season precipitation over the Yanshan–Taihangshan Mountain ranges along the east peripheries of the Loess and Inner Mongolian Plateaus and the adjacent North China Plains using the high-resolution CMORPH precipitation data during May–August of 2003–09. Warm-season rainfalls account for nearly 80% of the total precipitation in this focus area and thus have very important impacts on the water cycles and climate of a region encompassing the capital city of Beijing and several of the most densely populated provinces of China.

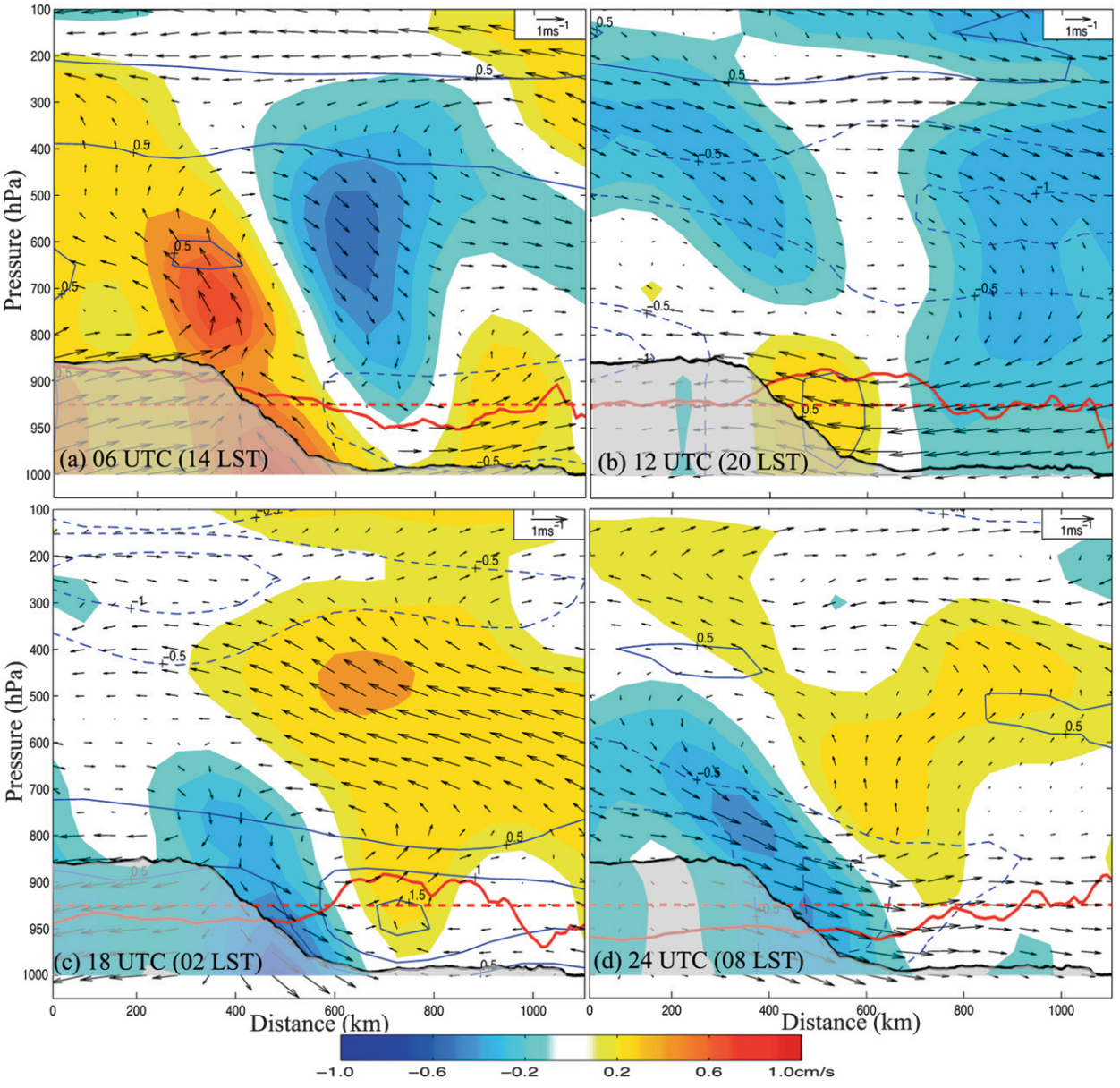

FIG. 6. Vertical profiles of the averaged vertical motion (colored; cm s^{-1}), the perturbation vertical circulation vectors (horizontal wind component along the cross section and 100 times the vertical velocity), and the horizontal wind component perpendicular to the cross section (contoured in blue every 0.5 m s^{-1}, where solid indicates southwesterlies and dashed indicates northwesterlies) along the direction from northwest to southeast averaged as in Figs. 1c and 4 diagnosed with the GFS analyses at (a) 0600, (b) 1200, (c) 1800, and (d) 0000 UTC. The red solid curves show the averaged normalized diurnal precipitation deviation, with the red dashed straight line as the zero value. Analysis fields below the ground are masked with light-gray shadings.

It is found that the peak in the local precipitation usually begins near midday or early afternoon (time of maximum solar heating) on the southeastern slopes of the plateaus and propagates southeastward at a speed of ~13 m s^{-1}. The primary diurnal precipitation peak reaches the central North China Plains around midnight and the early morning hours. Two mechanisms are likely responsible for the nocturnal precipitation maximum over the North China Plains: 1) the initiation or enhancement of precipitation events during peak solar heating hours on the eastern slopes of the plateaus, which subsequently propagate southeastward to the plains, following the mid-tropospheric mean flow, and 2) the local initiation or enhancement of precipitation following the upward branch of a mountain–plain solenoidal circulation induced by differential heating between the mountain ranges and

plains, which is further facilitated by the nocturnal low-level jet over the plains that contributes to a transport of warm, moist air to the area during nighttime.

Future studies will examine the respective contributions from each of these two likely mechanisms, as well as the importance of the midtropospheric mean flow and/or the cold-pool dynamics for further explaining the near-continuous propagation of diurnal precipitation peaks from high terrains to the plains in this area, through both case studies of individual events and idealized simulations, as in Trier et al. (2006, 2010) for the continental United States.

Acknowledgments. We are grateful to Pingping Xie and Soo-Hyun Yoo for providing the CMORPH dataset, for proofreading by Thomas Hinson and Jon Poterjoy, and for comments from Rit Carbone, Aiguo Dai, Tianjun Zhou, Juan Fang, and two anonymous reviewers. This research was jointly sponsored by a special fund allocated for Basic Research and Operation from the Chinese Academy of Meteorological Sciences (2008Z002) and the National Key Project of China for Developing Basic Sciences (2004CB418307), and U.S. National Science Foundation Grants ATM-0618662 and ATM-0904635.

REFERENCES

Bonner, W. D., 1968: Climatology of the low-level jet. *Mon. Wea. Rev.,* **96,** 833–850.

Carbone, R. E., and J. D. Tuttle, 2008: Rainfall occurrence in the U.S. warm season: The diurnal cycle. *J. Climate,* **21,** 4132–4146.

——, ——, D. Ahijevych, and S. B. Trier, 2002: Inferences of predictability associated with warm season precipitation episodes. *J. Atmos. Sci.,* **59,** 2033–2056.

Chen, G., W. Sha, and T. Iwasaki, 2009: Diurnal variation of precipitation over southeastern China: Spatial distribution and its seasonality. *J. Geophys. Res.,* **114,** D13103, doi:10.1029/2008JD011103.

Dai, A., F. Giorgi, and K. E. Trenberth, 1999: Observed and model simulated precipitation diurnal cycle over the contiguous United States. *J. Geophys. Res.,* **104,** 6377–6402.

——, X. Lin, and K.-L. Hsu, 2007: The frequency, intensity, and diurnal cycle of precipitation in surface and satellite observations over low- and mid-latitudes. *Climate Dyn.,* **29,** 727–744.

Higgins, R. W., Y. Yao, E. S. Yarosh, J. E. Janowiak, and K. C. Mo, 1997: Influence of the Great Plains low-level jet on summertime precipitation and moisture transport over the central United States. *J. Climate,* **10,** 481–507.

Janowiak, J. E., V. E. Kousky, and R. J. Joyce, 2005: Diurnal cycle of precipitation determined from the CMORPH high spatial and temporal resolution global precipitation analyses. *J. Geophys. Res.,* **110,** D23105, doi:10.1029/2005JD006156.

Joyce, R. J., J. E. Janowiak, P. A. Arkin, and P. Xie, 2004: CMORPH: A method that produces global precipitation estimates from passive microwave and infrared data at high spatial and temporal resolution. *J. Hydrometeor.,* **5,** 487–503.

Koch, S. E., F. Zhang, M. L. Kaplan, Y.-L. Lin, R. Weglarz, and C. M. Trexler, 2001: Numerical simulations of a gravity wave event over CCOPE. Part III: The role of a mountain–plains solenoid in the generation of the second wave episode. *Mon. Wea. Rev.,* **129,** 909–933.

Lin, Y., and F. Zhang, 2008: Tracking mesoscale gravity waves in baroclinic jet-front systems. *J. Atmos. Sci.,* **65,** 2402–2415.

Qian, W., H. Kang, and D. Lee, 2002: Distribution of seasonal rainfall in East Asian Monsoon region. *Theor. Appl. Climatol.,* **73,** 151–168.

Trier, S. B., C. A. Davis, D. A. Ahijevych, M. L. Weisman, and G. H. Bryan, 2006: Mechanisms supporting long-lived episodes of propagating nocturnal convection within a 7-day WRF model simulation. *J. Atmos. Sci.,* **63,** 2437–2461.

——, ——, and ——, 2010: Environmental controls on the simulated diurnal cycle of warm-season precipitation in the continental United States. *J. Atmos. Sci.,* in press.

Tripoli, G. J., and W. R. Cotton, 1989: Numerical study of an observed orogenic mesoscale convective system. Part II: Analysis of governing dynamics. *Mon. Wea. Rev.,* **117,** 305–328.

Wallace, J. M., 1975: Diurnal variations in precipitation and thunderstorm frequency over the conterminous United States. *Mon. Wea. Rev.,* **103,** 406–419.

Wang, C. C., G. T. J. Chen, and R. E. Carbone, 2004: A climatology of warm-season cloud patterns over east Asia based on GMS infrared brightness temperature observations. *Mon. Wea. Rev.,* **132,** 1606–1629.

Wolyn, P. G., and T. B. McKee, 1994: The mountain–plains circulation east of a 2-km-high north–south barrier. *Mon. Wea. Rev.,* **122,** 1490–1508.

Yin, S., D. Chen, and Y. Xie, 2009: Diurnal variations of precipitation during the warm season over China. *Int. J. Climatol.,* **29,** 1154–1170.

Yu, R., T. Zhou, and A. Xiong, 2007: Diurnal variation of summer precipitation over contiguous China. *Geophys. Res. Lett.,* **34,** L01704, doi:10.1029/2006GL028129.

Zhang, F., and S. E. Koch, 2000: Numerical simulation of a gravity wave event observed during CCOPE. Part II: Wave generation by an orographic density current. *Mon. Wea. Rev.,* **128,** 2777–2796.

Zhou, T., R. Yu, H. Chen, A. Dai, and Y. Pan, 2008: Summer precipitation frequency, intensity, and diurnal cycle over China: A comparison of satellite data with rain gauge observations. *J. Climate,* **21,** 3997–4010.